

Observation of distinct Kondo effect and anomalous Hall effect in V self-intercalated layered antiferromagnet V_5S_8 crystals

Yaofeng Xie(谢耀锋), Senhao Lv(吕森浩), Qi Qi(齐琦), Guojing Hu(胡国静), Ke Zhu(祝轲), Zhen Zhao(赵振), Guoyu Xian(冼国裕), Yechao Han(韩烨超), Ruwen Wang(王汝文), Chenyu Bai(白晨宇), Lihong Bao(鲍丽宏), Xiao Lin(林晓), Hui Guo(郭辉), Haitao Yang(杨海涛), and Hong-Jun Gao(高鸿钧)

Citation: Chin. Phys. B, 2025, 34 (**8**): 087303. DOI: 10.1088/1674-1056/add5cd
http://cpb.iphy.ac.cn; http://iopscience.iop.org/cpb

What follows is a list of articles you may be interested in

Manipulating the magnetic properties of $MnBi_2Te_4$ through electrochemical organic molecule intercalation

Yu Du(杜钰), Heng Zhang(张恒), Fuwei Zhou(周福伟), Tianqi Wang(王天奇), Jiajun Li(李佳骏), Wuyi Qi(戚无逸), Yiying Zhang (张祎颖), Yefan Yu(俞业凡), Fucong Fei(费付聪), and Fengqi Song(宋凤麒)

Chin. Phys. B, 2025, 34 (**8**): 087302. DOI: 10.1088/1674-1056/add5cf

In-plane negative magnetoresistance and quantum oscillations in van der Waals antiferromagnet $DyTe_3$

Qi Qi(齐琦), Senhao Lv(吕森浩), Ke Zhu(祝轲), Yaofeng Xie(谢耀锋), Guojing Hu(胡国静), Zhen Zhao(赵振), Guoyu Xian(冼国裕), Yechao Han(韩烨超), Yang Yang(杨洋), Lihong Bao(鲍丽宏), Xiao Lin(林晓), Hui Guo(郭辉), Haitao Yang(杨海涛), and Hong-Jun Gao(高鸿钧)

Chin. Phys. B, 2025, 34 (**7**): 077305. DOI: 10.1088/1674-1056/adcc87

Role of symmetry in antiferromagnetic topological insulators

Sahar Ghasemi and Morad Ebrahimkhas

Chin. Phys. B, 2025, 34 (**7**): 077302. DOI: 10.1088/1674-1056/adcb1e

Strain-modulated antiferromagnetic Chern insulator in $NiOsCl_6$ monolayer

Bin Wu(武斌), Na Li(李娜), Xin-Lian Chen(陈新莲), Wei-Xiao Ji(纪维霄), Pei-Ji Wang(王培吉), Shu-Feng Zhang(张树峰), and Chang-Wen Zhang(张昌文)

Chin. Phys. B, 2024, 33 (**12**): 127301. DOI: 10.1088/1674-1056/ad84cb

Negative magnetoresistance in the antiferromagnetic semimetal $V_{1/3}TaS_2$

Zi Wang(王子), Xin Peng(彭馨), Shengnan Zhang(张胜男), Yahui Su(苏亚慧), Shaodong Lai(赖少东), Xuan Zhou(周旋), Chunxiang Wu(吴春翔), Tingyu Zhou(周霆宇), Hangdong Wang(王杭栋), Jinhu Yang(杨金虎), Bin Chen(陈斌), Huifei Zhai(翟会飞), Quansheng Wu(吴泉生), Jianhua Du(杜建华), Zhiwei Jiao(焦志伟), and Minghu Fang(方明虎)

Chin. Phys. B, 2024, 33 (**3**): 037301. DOI: 10.1088/1674-1056/ad18aa

---

RAPID COMMUNICATION

Observation of distinct Kondo effect and anomalous Hall effect in V self-intercalated layered antiferromagnet V_5S_8 crystals

Yaofeng Xie(谢耀锋)[1,2,†], Senhao Lv(吕森浩)[1,†], Qi Qi(齐琦)[1,2], Guojing Hu(胡国静)[1], Ke Zhu(祝轲)[1,2], Zhen Zhao(赵振)[1], Guoyu Xian(冼国裕)[3], Yechao Han(韩烨超)[2], Ruwen Wang(王汝文)[1,2], Chenyu Bai(白晨宇)[1,2], Lihong Bao(鲍丽宏)[1,2], Xiao Lin(林晓)[2], Hui Guo(郭辉)[1,2,‡], Haitao Yang(杨海涛)[1,2,§], and Hong-Jun Gao(高鸿钧)[1,2]

[1] *Beijing National Center for Condensed Matter Physics and Institute of Physics, Chinese Academy of Sciences, Beijing* 100190, *China*
[2] *School of Physical Sciences, University of Chinese Academy of Sciences, Beijing* 100049, *China*
[3] *Songshan Lake Materials Laboratory, Dongguan* 523808, *China*

(Received 24 March 2025; revised manuscript received 20 April 2025; accepted manuscript online 8 May 2025)

Vanadium-based transition metal chalcogenides V_mX_n (X = S, Se, Te) with their distinctive quantum effects, tunable magnetism, spin–orbit coupling, and high carrier mobility are a valuable platform to explore the interplay between magnetism and electronic correlations, especially with tunable structural phases and magnetic properties through stoichiometric variations, making them ideal candidates for advanced device applications. Here, we report the synthesis of high-quality $V_{5+x}S_8$ single crystals with different concentrations of self-intercalated vanadium. $V_{5+x}S_8$ crystals show an antiferromagnetic behavior and a spin-flop-like transition below T_N of 30.6 K. The high-quality $V_{5+x}S_8$ single crystals exhibit a large negative magnetoresistance of 12.3% at 2 K. Interestingly, $V_{5+x}S_8$ crystals show an obvious low-temperature resistance upturn that gradually levels off with the increasing magnetic field, attributed to the Kondo effect arising from the interaction between conduction electrons and embedded vanadium magnetic impurities. With increasing V doping, the antiferromagnetic interactions intensify, weakening the coupling between the local moments and conduction electrons, which in turn lowers the Kondo temperature (T_K). Furthermore, the anomalous Hall effect is observed in $V_{5.73}S_8$, with an anomalous Hall conductivity (AHC) of 50.46 $\Omega^{-1}\cdot cm^{-1}$ and anomalous Hall angle of 0.73% at 2 K. Our findings offer valuable insights into the mechanisms of the Kondo effect and anomalous Hall effect in self-intercalated transition metal chalcogenides with complex magnetism and electronic correlation effects.

Keywords: $V_{5+x}S_8$ crystals, antiferromagnetic, negative magnetoresistance, Kondo effect, anomalous Hall effect

PACS: 73.43.Qt

DOI: 10.1088/1674-1056/add5cd **CSTR:** 32038.14.CPB.add5cd

1. Introduction

Two-dimensional (2D) layered materials, with weak interlayer interactions, display unique quantum effects, spin–orbit coupling, tunable band gaps, and high electron mobility, making them highly promising for applications in spintronics, nanoelectronics and topological quantum computing.[1–8] Of particular interest, 2D layered magnetic materials, which retain intrinsic long-range magnetic order down to the atomic-level thickness, are considered excellent platforms for exploring low-dimensional magnetism and electronic correlation effects, offering tunable properties for applications in spintronics devices and non-volatile memory.[9–14] A topological Hall effect signal with antisymmetric peaks in layered ferromagnetic $Cr_{1.2}Te_2$ suggests spin chirality due to spin canting under external magnetic fields,[15] showing potential for chiral spin-based van der Waals spintronics devices. Moreover, room-temperature asymmetric magnetoresistance was observed in ferromagnetic Fe_3GaTe_2 nano-device due to the planar symmetry breaking,[16] showing three resistance states under varying magnetic fields for possible multi-state memory and logic applications. Therefore, further investigating new 2D layered magnetic materials and understanding their underlying magnetoelectronic transport mechanism are essential for advancing the development of 2D spintronics devices.

Recently, vanadium-based transition metal chalcogenides with the chemical formula V_mX_n (X = S, Se, Te) have provided an excellent platform to explore the interplay between the magnetism and electron correlation effect, especially with tunable structural phases and magnetic properties through stoichiometric variations.[17–19] Significant room-temperature ferromagnetism has been observed in monolayer VSe_2 grown on van der Waals substrates (such as graphite and MoS_2).[20] And 1T phase multilayer VTe_2 nanoplates grown via CVD exhibit the Kondo effect, which is attributed to the localized mag-

†These authors contributed equally to this work.
‡Corresponding author. E-mail: guohui@iphy.ac.cn
§Corresponding author. E-mail: htyang@iphy.ac.cn

© 2025 Chinese Physical Society and IOP Publishing Ltd. All rights, including for text and data mining, AI training, and similar technologies, are reserved.

netic moments from interstitial vanadium ions.[21] By engineering the van der Waals interactions in 2D vanadium disulfide (VS_2), both spin properties and the bandgap can be precisely controlled, along with the development of intrinsic ferromagnetism and a narrow bandgap.[22] Interestingly, large sulfur vacancies can induce the transition of VS_2 from the 2*H* phase to the 1*T* phase, forming V_5S_8, where some vanadium atoms insert into the van der Waals spaces between layers, altering the crystal structure and physical properties.[23,24] In V_5S_8, the system predominantly exhibits an antiferromagnetic state, with a thickness-dependent magnetic order, and potential for nonzero Berry curvature or exotic surface states due to spin–lattice–electron interactions.[25–27] Hence, antiferromagnetic V_5S_8 with the unique lattice structure and tunable magnetism, which is crucial for understanding the interplay between magnetism and electronic correlation effects, should be further explored.

In this article, we report the synthesis of $V_{5+x}S_8$ single crystals with different concentrations of self-intercalated vanadium by the chemical vapor transport approach (CVT) using I_2 as the transport agent. Magnetic measurements reveal an antiferromagnetic transition in $V_{5+x}S_8$ at ~ 30.6 K, along with a spin-flop-like transition under a critical field of ~ 3 T in the low-temperature range of 2 K to 20 K. Low-temperature electrical transport measurements reveal that $V_{5.18}S_8$ crystals exhibit a large negative magnetoresistance of 12.3% at 2 K under an applied magnetic field of 9 T. Interestingly, below the critical temperature, $V_{5+x}S_8$ crystals exhibit an obvious resistance upturn that gradually levels off with increasing magnetic field, which is attributed to the Kondo effect arising from the interaction between conduction electrons and intercalated vanadium magnetic impurities. Remarkably, the anomalous Hall effect (AHE) is observed in $V_{5.73}S_8$ crystals, with an anomalous Hall conductivity (AHC) of 50.46 $\Omega^{-1}\cdot cm^{-1}$and anomalous Hall angle (AHA) of 0.73% at 2 K, respectively. Our work provides a valuable platform for understanding the mechanisms of the Kondo effect and anomalous Hall effect in vanadium-based transition metal chalcogenides, which is useful to explore the new spintronics devices with the complex magnetism and electronic interaction effects in self-intercalated layered materials.

2. Experimental method

Synthesis method The $V_{5+x}S_8$ single crystals were successfully synthesized by a chemical vapor transport approach,[25] as shown in Fig. S1. First, the raw materials V and S were mixed in a molar ratio of $V:S = 5+x:8$ and sealed together with the transport agent I_2 in a quartz tube under a high vacuum using a high-temperature flame gun. Then, the growth of the regular-shaped $V_{5+x}S_8$ single crystals was performed in a temperature gradient from 680 °C to 600 °C for about a week.

Sample characterizations XRD patterns were acquired by a Rigaku SmartLab SE x-ray diffractometer with Cu $K\alpha$ radiation ($\lambda = 0.15418$ nm) at room temperature. Crystal diffraction patterns were recorded with a Bruker D8 VentureSingle. Scanning electron microscopy (SEM) and x-ray energy-dispersive spectroscopy (EDS) were performed using a HITACHI S5000 equipped with a Bruker XFlash 6|60 energy dispersive analysis system. Magnetization measurements were conducted on single crystals using a vibrating sample magnetometer (MPMS 3, Quantum Design). Electrical transport measurements were carried out with a Quantum Design physical properties measurement system (PPMS).

3. Structure characterizations of V_5S_8 single crystals

V_5S_8 is a layered material that can be viewed as VS_2 intercalated with additional V atoms, crystallizing in a monoclinic structure with lattice parameters $a = 11.377$ Å, $b = 6.648$ Å, $c = 11.291$ Å, $\alpha = \gamma = 90°$, and $\beta = 91.45°$, belonging to the space group *F2/m*.[28–30] Vanadium intercalation induces a distorted 1*T* phase in VS_2 layers, creating structural complexity with three inequivalent V sites designated as V(1), V(2), and V(3), as shown in Fig. 1(a), where the intercalated V atoms mainly occupy V(1) sites, forming a slightly distorted triangular lattice. The intercalated V atoms distort the octahedral coordination of VS_2 layers, directly giving rise to an antiferromagnetic order, with spins aligning at a 10.4° angle from the *c*-axis due to the induced structural perturbations. The x-ray diffraction (XRD) pattern displays only the (00*l*) diffraction peaks (Fig. S2), confirming the pure phase of the as-grown V_5S_8 and its preferred [001] orientation. The rocking curve from the (002) reflection (Fig. 1(b)) exhibits a remarkably small full-width at half-maximum (FWHM) of $\sim 0.088°$, indicating the high crystalline quality of the as-grown V_5S_8 crystals. The inset of Fig. 1(b) presents an optical photograph of a typical V_5S_8 single crystal, showing a regular shape with a lateral dimension of 4 mm. And the (*h*0*l*) plane diffraction pattern exhibits sharp, unsplit diffraction spots (Fig. 1(c)), also verifying the high quality of the as-grown V_5S_8 single crystals. The high-resolution transmission electron microscopy (HRTEM) images and selected area electron diffraction (SAED) pattern shown in Fig. S3(a) reveal a lattice spacing of 0.266 nm, which corresponds to the (012) plane of V_5S_8.

Meanwhile, we prepared samples with different concentrations of self-intercalated vanadium and performed elemental analysis on each sample using SEM-EDS. The color maps of V and S show the uniform distribution of elements on the surface (Fig. S3(b)), and EDS measurements from multiple regions indicate that the V:S chemical ratios of samples S1–S4 are approximately 5.04:8, 5.18:8, 5.43:8, and 5.73:8, re-

spectively, as shown in Fig. S3(c). Subsequently, atomic-scale analysis was conducted on cross-sectional samples using aberration-corrected scanning transmission electron microscopy (STEM) to further evaluate the quality of the synthesized V_5S_8 single crystals. The STEM high-angle annular dark-field (HAADF) image and annular bright-field (ABF) images of V_5S_8 along the [001] axis, with an overlaid structural model, reveal a clean *ab*-plane with a hexagonal lattice structure (Figs. 1(d) and 1(e)). In addition, the HAADF and ABF images of V_5S_8 along the [100] axis, acquired simultaneously, show an impeccable crystalline structure with no visible defects (Figs. 1(f) and 1(g)).

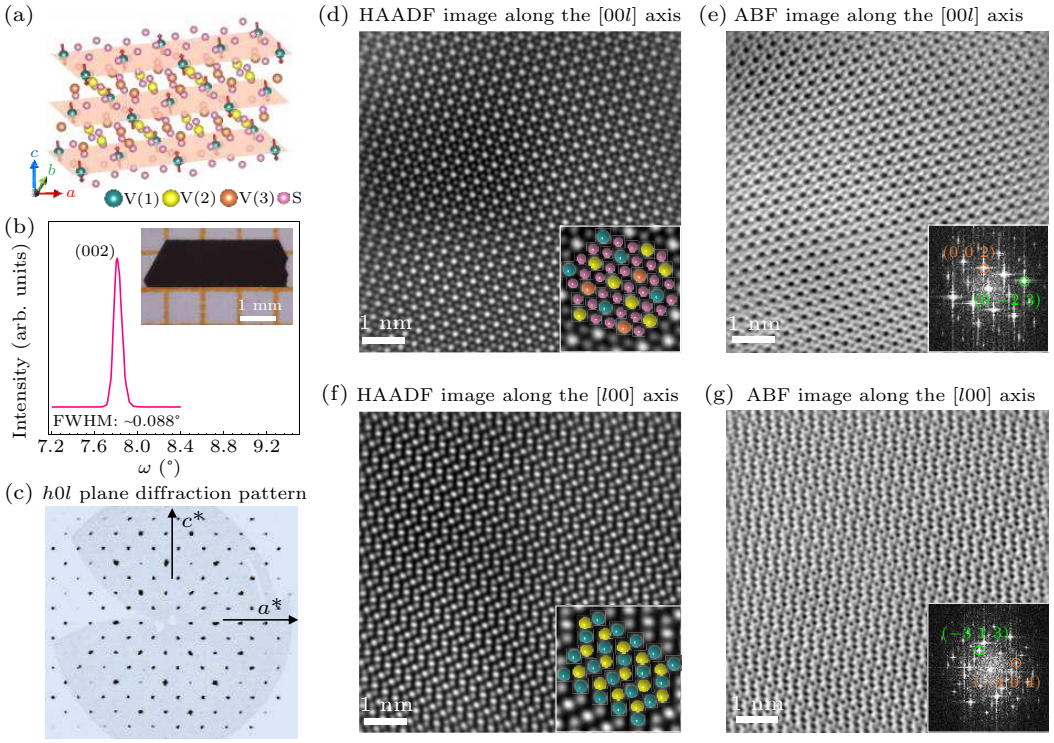


Fig. 1. Crystal structure characterization of V_5S_8 crystals. (a) The crystal structure of V_5S_8 extending across two-unit cells. The green-colored atoms represent intercalated vanadium atoms within the van der Waals gap between two VS_2 layers, contributing to the magnetic moments. (b) The x-ray rocking curve of the (002) reflection for the V_5S_8 single crystal, exhibiting a relatively small FWHM of $\sim 0.088°$. The upper inset presents the x-ray diffraction pattern and the lower inset displays an optical photograph of the V_5S_8 single crystal. (c) The (*h*0*l*) plane diffraction patterns of the V_5S_8 single crystal, showing sharp diffraction spots without splitting. (d) and (e) High-resolution HAADF and ABF images of the V_5S_8 single crystal along the [00*l*] zone axis. (f) and (g) High-resolution HAADF and ABF images of the V_5S_8 single crystal along the [*l*00] zone axis.

4. Magnetic properties and magnetoresistance of V_5S_8 single crystals

V_5S_8 is a layered van der Waals antiferromagnetic (AFM) material, with its magnetism primarily originating from the intercalated V atoms between the layers.[28–30] The temperature dependence of magnetization of $V_{5+x}S_8$ single crystals under a field of 0.1 T with the magnetic field (B) along the c axis, as shown in Fig. 2(a), reveals an antiferromagnetic transition around 30.6 K (T_N), with distinct magnetization values observed in $V_{5+x}S_8$ single crystals with different concentrations of self-intercalated vanadium, primarily attributed to the modification of the interlayer magnetic exchange coupling interaction. The field dependence of magnetization (M–H) with the field along the c-axis at 2 K shows the spin-flop (SF) like transitions in $V_{5+x}S_8$ single crystals with different concentrations of self-intercalated vanadium (Fig. 2(b)), in agreement with the previous reported results,[25,28–31] with the critical fields and the sharpness of the spin-flop transitions showing differences among the four samples. Figure 2(c) displays the field dependence of magnetization of $V_{5.04}S_8$ with $B \| c$ at different temperatures ranging from 2 K to 50 K, showing the spin-flop transitions below 20 K, while exhibiting a distinct paramagnetic behavior above 20 K.

The temperature dependence of the resistivity of $V_{5+x}S_8$ single crystals with different concentrations of self-intercalated vanadium under 0 T shows a metallic behavior from 2 K to 300 K (Fig. 2(d)). The first derivative of the resistivity ($\mathrm{d}\rho/\mathrm{d}T$) for $V_{5.04}S_8$, $V_{5.18}S_8$, $V_{5.43}S_8$ and $V_{5.73}S_8$ crystals plotted as a function of temperature, exhibits a drastic change in the slope around 30.2 K, corresponding to the antiferromagnetic transition (the inset of Fig. 2(d) and Figs. S4(a)–S4(d)). Interestingly, a negative slope in $\mathrm{d}\rho/\mathrm{d}T$ is observed at low temperatures for all four samples (highlighted by the dashed circles), indicating that the resistivity increases as the temperature decreases. The magnetic-field dependent magnetoresistance ($\mathrm{MR} = [\rho_{xx}(\mu_0 H) - \rho_{xx}(0)]/\rho_{xx}(0) \times 100\%$) for $V_{5+x}S_8$ single crystals with different concentrations of self-intercalated vanadium at different temperatures from 2 K to 50 K exhibits a nonsaturating negative magnetoresistance be-

havior (Fig. 2(e)), with the maximum negative MR reaching 12.3% at 9 T for $V_{5.18}S_8$, which is higher than previously reported values in the literature.[28–30] And the magnetoresistance remains nearly constant at low fields before abruptly dropping at ∼ 3 T due to the spin-flop transition, followed by a quadratic dependence on the magnetic field under high fields (Figs. S4(e) and S4(f)). Figure 2(f) shows the magnetic-field dependent magnetoresistance of $V_{5.04}S_8$ at various temperatures from 2 K to 100 K with $B \perp I$, where a kink at 3.0 T below T_N is attributed to a spin-flop transition,[28,29] and the negative magnetoresistance effect weakens with increasing temperature. To further investigate the effect of magnetic field orientation on resistivity, we examined the magnetoresistance (MR) over an angle range from 0° to 90°, with the magnetic field rotating in the z–x plane (Fig. S5(a)). The angular dependence of the out-of-plane AMR at different temperatures from 2 K to 50 K shows the two-fold symmetry under 2 T (Fig. S5(b)), with an anisotropy value of 0.2% at 10 K. Figure S5(c) shows the angular dependence of the out-of-plane AMR under 2 T and 9 T, where a noticeable phase shift in the AMR is observed between low and high magnetic fields, which may be attributed to spin-flop transitions.

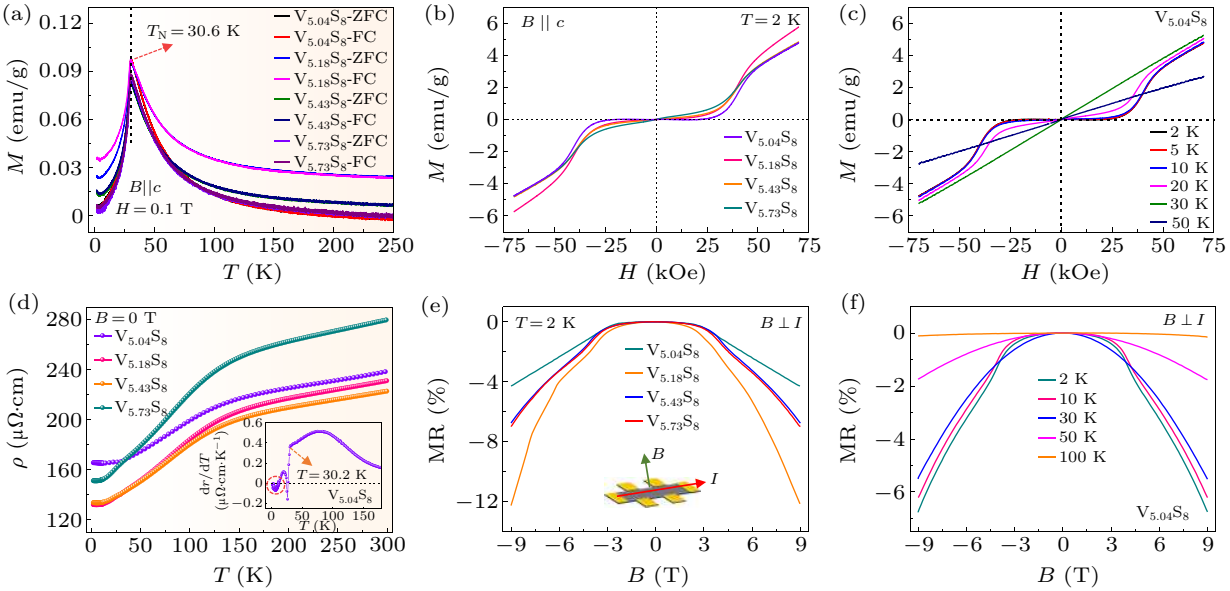


Fig. 2. Magnetism and magnetoresistance of $V_{5+x}S_8$ crystals. (a) Temperature dependence of magnetization with ZFC and FC procedures of $V_{5+x}S_8$ crystals under 0.1 T, showing an antiferromagnetic transition (T_N) around 30.6 K. (b) The field dependence of the magnetization of $V_{5+x}S_8$ crystals at 2 K, displaying a spin-flop-like transition around ∼ 3 T. (c) The field dependence of the magnetization of $V_{5.04}S_8$ crystals at different temperatures from 2 K to 50 K. (d) Temperature dependence of the resistivity of $V_{5+x}S_8$ crystals under 0 T. The inset shows the first derivative of the resistivity ($d\rho/dT$) for $V_{5.04}S_8$ crystals plotted as a function of temperature. (e) Magnetoresistance of $V_{5+x}S_8$ crystals under different applied fields up to 9 T at 2 K for $B \perp I$, exhibiting a non-saturated negative magnetoresistance behavior. (f) The field dependence of the magnetoresistance of $V_{5.04}S_8$ crystals at different temperatures ranging from 2 K to 100 K, with a maximum negative magnetoresistance of 6.8% at 2 K under 9 T.

5. Kondo effect of $V_{5+x}S_8$ single crystals

Subsequently, we focused on the low-temperature resistivity upturn behavior. Generally, there are three likely microscopic mechanisms contributing to the resistivity upturn at low temperatures, i.e., (i) electron–electron interaction,[32] (ii) weak localization,[33] and (iii) the Kondo effect,[34] with electron–electron interaction leading to positive MR,[35] while the Kondo effect and weak localization result in negative MR.[21] Additionally, as the applied magnetic field increases, the resistivity minima are suppressed in the Kondo effect and weak localization, while electron–electron interactions remain unaffected. In the case of $V_{5+x}S_8$ single crystals, a negative MR is observed (Figs. 2(e) and 2(f)), and with increasing applied magnetic field, the resistivity upturn is suppressed (Fig. S6), thereby ruling out the influence of electron–electron interactions. Weak localization (WL) and weak antilocalization (WAL) effects are commonly observed in low-dimensional systems, such as thin films and nanowires,[36,37] due to enhanced scattering that leads to quantum interference.[38] In low magnetic fields, WL induces characteristic features in the resistance, typically manifesting as a peak near zero field. Moreover, as the magnetic field increases, the effect of weak localization gradually diminishes due to the disruption of quantum interference by stronger magnetic fields.[38,39] In our case, the absence of a cusp-like feature in the low-field region of the magnetoresistance curve, along with the fact that the Kondo effect typically induces negative magnetoresistance with a quadratic field dependence, allows us to rule out the influence of WL. Consequently, we attribute the low-temperature resistivity upturn in V_5S_8 primarily to the Kondo effect, originating from the interaction between conduction electrons and intercalated vanadium magnetic impurities.

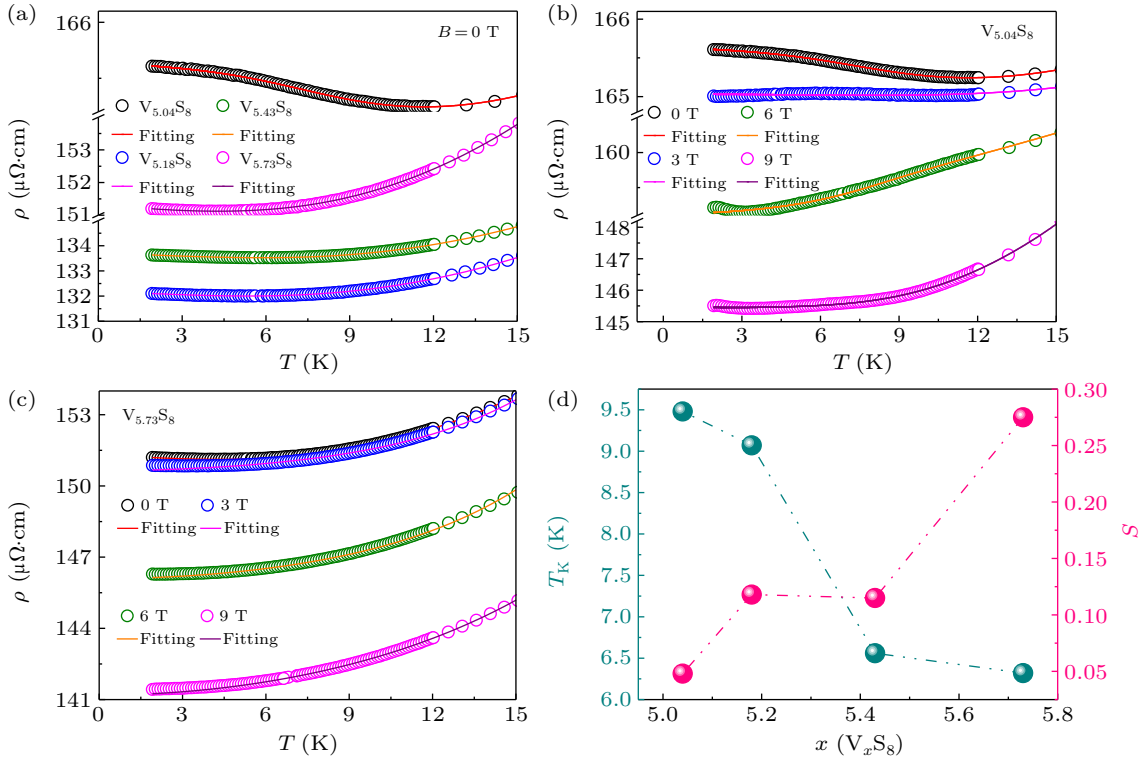


Fig. 3. Low-temperature resistivity of $V_{5+x}S_8$ crystals. (a) The logarithmic low-temperature dependence of resistivity for $V_{5.04}S_8$, $V_{5.18}S_8$, $V_{5.43}S_8$ and $V_{5.73}S_8$ crystals without an applied magnetic field, where solid lines represent the fits to the Kondo model. (b) and (c) The logarithmic low-temperature dependence of resistivity for $V_{5.04}S_8$ and $V_{5.73}S_8$ crystals under 0 T, 3 T, 6 T, and 9 T, respectively. (d) V content dependence of the fitted Kondo temperature T_K and the spin S of the magnetic impurities, showing that as the V content increases, the Kondo temperature gradually decreases, while the spin gradually increases.

The low-temperature logarithmic upturn in resistivity can be effectively described within the framework of the Kondo effect. The resistivity in the temperature range of 2 to 10 K is well fitted by the following equation:[21,40]

$$\rho(T) = \rho_0 + qT^2 + pT^5 + \rho_{K0}\left\{1 - \ln\left(\frac{T}{T_K}\right) \times \left[\ln^2\left(\frac{T}{T_K}\right) + S(S+1)\pi^2\right]^{-1/2}\right\}, \quad (1)$$

where ρ_0 corresponds to the residual resistivity, qT^2 accounts for the Fermi liquid contribution, pT^5 represents the electron–phonon contribution, and the fourth term describes the Kondo resistivity, which follows the Hamann expression. Here, ρ_{K0} is the temperature-independent resistivity, T_K denotes the Kondo temperature, and S represents the spin of the magnetic impurities. Figure 3(a) displays the logarithmic low-temperature dependence of resistivity for $V_{5.04}S_8$, $V_{5.18}S_8$, $V_{5.43}S_8$ and $V_{5.73}S_8$ crystals without an applied magnetic field from 2 K to 10 K, in which hollow circles with different colors and solid lines represent the experimental data and the fitting curve, demonstrating a good fit to the experimental data. The low-temperature resistivity of $V_{5.04}S_8$, $V_{5.18}S_8$, $V_{5.43}S_8$ and $V_{5.73}S_8$ crystals under 0 T, 3 T, 6 T, and 9 T (Figs. 3(b), 3(c) and S6) reveals that upon applying a magnetic field, a broad peak appears, and the resistivity curve progressively flattens with increasing field, indicating the suppression of the Kondo effect. This behavior reflects the splitting of the Kondo resonance under the influence of the applied magnetic field. The temperature-dependent resistivity at different magnetic fields is fitted using Eq. (1) incorporating a modified Hamann term[21,41]

$$\rho(T) = \rho_0 + qT^2 + pT^5 + \rho_{K0}\left\{1 - \ln\left(\frac{T}{T_K}\right) \times \left[\ln^2\left(\frac{T}{T_K}\right) + S(S+1)\pi^2\right]^{-1/2}\right\} \times \left\{1 - B^2\left[\frac{g\mu_B H}{k_B(T+T_K)}\right]\right\}. \quad (2)$$

Here, $B(x)$ represents the Brillouin function for $S = 1/2$, $B(x) = \frac{2S+1}{2S}\coth\left(\frac{2S+1}{2S}x\right) - \frac{1}{2S}\coth\left(\frac{1}{2S}x\right)$, S stands for the spin of the magnetic impurity, g denotes the Landé g-factor (with a value of $g = 2$), μ_B stands for the Bohr magneton, while k_B refers to the Boltzmann constant.

The fitting results (Fig. S7) show that the Kondo temperatures T_K of $V_{5.04}S_8$, $V_{5.18}S_8$, $V_{5.43}S_8$, and $V_{5.73}S_8$ crystals are 9.48 K, 9.07 K, 6.56 K, and 6.32 K, respectively, while the spins S of the magnetic impurities are 0.048, 0.118, 0.115, and 0.275, respectively. Figure 3(d) shows the V content dependence of the fitted Kondo temperature T_K and the spin S of the magnetic impurities, showing that as the V content increases, the spin gradually increases, while the Kondo temperature gradually decreases. In a Kondo system, the impurity

spin (S) interacts with the conduction electron spin (r) of the host metal via an exchange interaction (J), whose sign dictates whether the coupling is antiferromagnetic (AFM) or ferromagnetic (FM). For $J < 0$ (AFM exchange), the system undergoes the Kondo screening, where the impurity spin and conduction electrons form a spin singlet state ($S_{\text{total}} = 0$). When the temperature drops below the Kondo temperature ($T < T_{\text{K}}$), the Kondo screening becomes fully established, effectively "hiding" the impurity magnetic moment.[42] In contrast, for $J > 0$ (FM exchange), conduction electrons tend to align parallel to the impurity spin, forming a locally polarized "screening cloud". In the low-temperature limit, the impurity spin becomes asymptotically free, preventing the formation of Kondo screening.[42–44] In $V_{5+x}S_8$ systems, V doping modifies the spin exchange interaction balance, with increasing V content strengthening AFM interactions, which tend to lock local magnetic moments, reducing their coupling with conduction electrons. As a result, the local moments in the system are increasingly constrained by antiferromagnetic (AFM) correlations, hindering their interaction with conduction electrons. This suppression of the Kondo screening leads to a decrease in the Kondo temperature (T_{K}), weakening the overall Kondo effect and diminishing the associated resistivity upturn typically observed at low temperatures.

6. Anomalous Hall effect of $V_{5.73}S_8$ crystals

Subsequently, we conducted a detailed study on the anomalous Hall signals observed in the Hall resistivity. For V_5S_8 system, the intercalated vanadium in the V (1) layer is the primary contributor to the system's magnetism. In its collinear antiferromagnetic (AF) ground state, the net magnetization is nearly zero, resulting in a negligible anomalous Hall effect (AHE). However, upon transitioning to a spin-flopped state, the increased magnetization enhances the AHE, driven by the delocalization effect of the flopped moments from the intercalated vanadium V site.[25] Figure 4(a) displays the magnetic-field dependence of Hall resistivity at different temperatures from 2 K to 100 K with $B \perp I$, exhibiting a pronounced nonlinear behavior below 30 K, primarily attributed to the contributions from both the normal Hall effect and the anomalous Hall effect, while above 30 K, the Hall resistivity shows a linear dependence on the magnetic field, mainly originating from the normal Hall effect. In general, the formula for Hall resistivity (ρ_{xy}) can be described as $\rho_{xy} = R_{\text{H}}B + \rho_{xy}^{\text{A}}$,[45] in which the first term is the normal Hall resistivity (ρ_{xy}^{N}) owing to the Lorentz effect. Figure 4(b) exhibits the magnetic-field dependence of anomalous Hall resistivity (ρ_{xy}^{A}) at different temperatures ranging from 2 K to 26 K, where ρ_{xy}^{N} is extracted through linear fitting of the high field part and ρ_{xy}^{A} is obtained by subtracting ρ_{xy}^{N}. It is observed that the anomalous Hall resistivity gradually decreases as the temperature increases, with the maximum value reaching 1.04 μΩ·cm at 2 K.

Next, we focus on two key parameters, the anomalous Hall conductivity σ_{xy}^{A} (AHC) and anomalous Hall angle (AHA). The Hall conductivity (σ_{xy}^{A}) and longitudinal conductivity (σ_{xx}) as the important characteristic parameters are

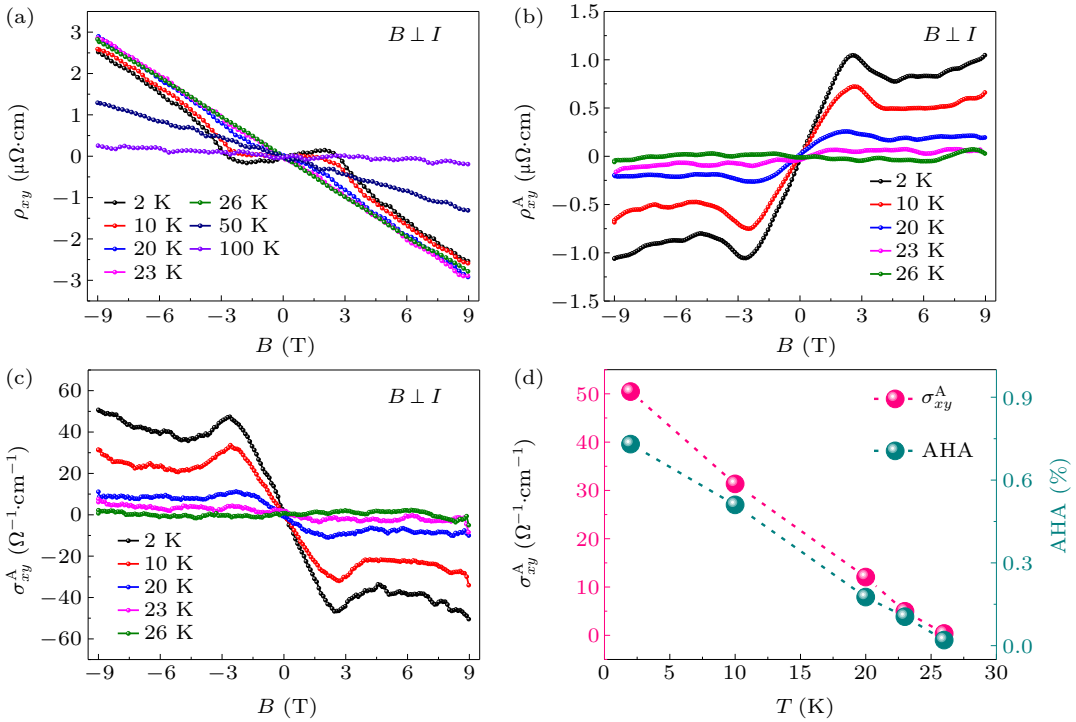


Fig. 4. Anomalous Hall effect of $V_{5.73}S_8$ crystals. (a) Field dependence of Hall resistivity at different temperatures from 2 K to 100 K. (b) Field dependence of the extracted anomalous Hall resistivity ρ_{xy}^{A} at different temperatures from 2 K to 26 K. (c) Field dependence of the anomalous Hall conductivity σ_{xy}^{A} from 2 K to 26 K. (d) Temperature dependence of σ_{xy}^{A} and AHA, showing a maximum conductivity value of 50.46 $\Omega^{-1}\cdot\text{cm}^{-1}$ and AHA value of 0.73% at 2 K.

given by $\sigma_{xy} = \frac{-\rho_{xy}}{\rho_{xy}^2+\rho_{xx}^2}$ and $\sigma_{xx} = \frac{\rho_{xx}}{\rho_{xy}^2+\rho_{xx}^2}$,[46,47] respectively, in which ρ_{xx} is the longitudinal resistivity, and the AHC σ_{xy}^{A} is obtained by subtracting the normal Hall conductivity σ_{xy}^{N}. Figure 4(c) shows the magnetic-field dependence of σ_{xy}^{A} at different temperatures from 2 K to 26 K, where σ_{xy}^{A} decreases with increasing temperature, reaching a maximum value of 50.46 $\Omega^{-1}\cdot\mathrm{cm}^{-1}$ at 2 K. Aside from a large AHC, the $V_{5.73}S_8$ crystals also show an anomalous Hall angle (AHA) defined by the ratio of $\sigma_{xy}^{\mathrm{A}}/\sigma_{xx}$, where AHA is another important parameter for scaling the AHE, which provides a foundation for the relative contribution of the anomalous Hall current to the longitudinal current. Figure 4(d) shows the temperature dependence of σ_{xy}^{A} and AHA, indicating that AHA decreases with increasing temperature, with a maximum AHA value of 0.73% at 2 K. The significant anomalous Hall effect in V_5S_8 highlights its decent magnetic transport properties, offering a promising prospect for exploring the spin transport mechanisms in self-intercalated vanadium-based transition metal chalcogenides.

7. Conclusion

In summary, we have successfully synthesized high-quality $V_{5+x}S_8$ single crystals with different concentrations of self-intercalated vanadium by using a CVT approach. Magnetic measurements show an antiferromagnetic transition in $V_{5+x}S_8$ around 30.6 K, as well as a spin-flop-like transition occurring under a critical field of $\sim$ 3 T below T_{N}. And the high-quality $V_{5.18}S_8$ single crystal exhibits a large negative magnetoresistance of 12.3% at 2 K under an applied magnetic field of 9 T. At low magnetic fields, the magnetoresistance remains nearly constant, decreases suddenly at $\sim$ 3 T due to spin-flop transitions below 30 K, and follows a quadratic dependence on the field at higher magnetic fields. Interestingly, $V_{5+x}S_8$ crystals show an obvious resistance upturn at low temperatures, which gradually levels off with increasing magnetic field, attributed to the Kondo effect arising from the interaction between conduction electrons and embedded vanadium magnetic impurities. As the V doping amount increases, the antiferromagnetic interactions strengthen, reducing the coupling between local moments and conduction electrons, which results in a decrease in the Kondo temperature (T_{K}). Remarkably, the anomalous Hall effect is observed in $V_{5.73}S_8$, with an anomalous Hall conductivity (AHC) of 50.46 $\Omega^{-1}\cdot\mathrm{cm}^{-1}$ and anomalous Hall angle of 0.73% at 2 K, respectively. Our findings provide significant insights into the mechanism of the Kondo effect and anomalous Hall effect in $V_{5+x}S_8$ crystal materials, advancing the exploration of potential spintronics devices with the complex magnetism and electronic interaction effects in self-intercalated layered materials.

Acknowledgments

Project supported by the National Key R&D Program of China (Grant No. 2022YFA1204100), the National Natural Science Foundation of China (Grant Nos. 62488201 and 1240041502), the CAS Project for Young Scientists in Basic Research (Grant No. YSBR-003), the Chinese Academy of Sciences (Grant No. XDB33030100), and the Innovation Program of Quantum Science and Technology (Grant No. 2021ZD0302700).

References

[1] Deng Y, Yu Y, Song Y, Zhang J, Wang N Z, Sun Z, Yi Y, Wu Y Z, Wu S, Zhu J, Wang J, Chen X H and Zhang Y 2018 *Nature* **563** 94
[2] Ali M N, Xiong J, Flynn S, Tao J, Gibson Q D, Schoop L M, Liang T, Haldolaarachchige N, Hirschberger M, Ong N P and Cava R J 2014 *Nature* **514** 205
[3] la Barrera S C, Sinko M R, Gopalan D P, Sivadas N, Seyler K L, Watanabe K, Taniguchi T, Tsen A W, Xu X D, Xiao D and Hunt B M 2018 *Nat. Commun.* **9** 1427
[4] Sun Z P, Martinez A and Wang F 2016 *Nat. Photonics* **10** 227
[5] Ng H K, Xiang D, Suwardi A, Hu G W, Yang K, Zhao Y S, Liu T, Cao Z H, Liu H J, Li S S, Cao J, Zhu Q, Dong Z G, Tan C K I, Chi D Z, Qiu C W, Hippalgaonkar K, Eda G, Yang M and Wu J 2022 *Nat. Electron.* **5** 489
[6] Novoselov K S, Mishchenko A, Carvalho A and Neto A H C2016 *Science* **353** aac9439
[7] Yi H M, Hu L H, Wang Y X, Xiao R, Cai J Q, Hickey D R, Dong C Y, Zhao Y F, Zhou L J and Zhang R X 2022 *Nat. Mater.* **21** 1366
[8] Li Y J, Yin R T, Li M Z, Gong J S, Chen Z Y, Zhang J K, Yan Y J and Feng D L 2024 *Nat. Commun.* **15** 10121
[9] Wang Z, Gibertini M, Dumcenco D, Taniguchi T, Watanabe K, Giannini E and Morpurgo A F 2019 *Nat. Nanotechnol.* **14** 1116
[10] Ghazaryan D, Greenaway M T, Wang Z, Guarochico-Moreira V H, Vera-Marun I J, Yin J, Liao Y, Morozov S V, Kristanovski O, Lichtenstein A I, Katsnelson M I, Withers F, Mishchenko A, Eaves L, Geim A K, Novoselov K S and Misra A 2018 *Nat. Electron.* **1** 344
[11] Zhang G, Guo F, Wu H, Wen X, Yang L, Jin W, Zhang W and Chang H 2022 *Nat. Commun.* **13** 5067
[12] Lee J U, Lee S, Ryoo J H, Kang S, Kim T Y, Kim P, Park C H, Park J G and Cheong H 2016 *Nano Lett.* **16** 7433
[13] Tian Y, Gao W, Henriksen E A, Chelikowsky J R and Yang L 2019 *Nano Lett.* **19** 7673
[14] Cao T F, Shao D F, Huang K, Gurung G and Tsymbal E Y 2023 *Nano Lett.* **23** 3781
[15] Huang M, Zhang Y, Lei X Y, Hu G J, Xiang J X, Zeng H L, Fu X W, Zhang Z M and Chai G Z 2021 *Nano Lett.* **21** 4280
[16] Hu G J, Guo H, Lv S H, Li L X, Wang Y H, Han Y C, Pan L L, Xie Y L, Yu W Q, Zhu K, Qi Q, Xian, G Y, Zhu S Y, Shi J A, Bao L H, Lin X, Zhou W, Yang H T and Gao H J 2024 *Adv. Mater.* **36** 2403154
[17] Wang Y, Sofer Z, Luxa J and Pumera M M 2016 *Adv. Mater. Interfaces* **3** 1600433
[18] Sugawara K, Nakata Y, Fujii K, Nakayama K, Souma S, Takahashi T and Sato T 2019 *Phys. Rev. B* **99** 241404
[19] Hardy W J, Yuan J T, Guo H, Zhou P P, Lou J and Natelson D 2016 *ACS Nano* **10** 5941
[20] Bonilla M, Kolekar S, Ma Y, Diaz H C, Kalappattil V, Das R, Eggers T, Gutierrez H R, Manh-Huong P and Batzill M 2018 *Nat. Nanotechnol.* **13** 289
[21] Liu H T, Xue Y Z, Sho J A, Guzman R A, Zhan P P, Zhou Z, He Y G, Bian C, Wu L M, Ma R S, Chen J C, Yan J H, Yang H T, Shen C M, Zhou W, Bao L H and Gao H J 2019 *Nano Lett.* **19** 8572
[22] Guo Y Q, Deng H T, Sun X, Li X L, Zhao J Y, Wu J C, Chu W S, Zhang S J, Pan H B, Zheng X S, Wu X J, Jin C Q, Wu C Z and Xie Y 2017 *Adv. Mater.* **29** 1700715
[23] Niu J J, Yan B M, Ji Q Q, Liu Z F, Li M Q, Gao P, Zhang Y F, Yu D P and Wu X S 2017 *Phys. Rev. B* **96** 075402
[24] Zhou Z, Zhao X X, Wu L M, Liu H T, Chen J C, Xi C Y, Wang Z S, Liu E K, Zhou W, Pennycook S J, Pantelides S T, Zhang X G, Bao L H and Gao H J 2022 *Phys. Rev. B* **105** 235433

[25] Wu X K, Wang B, Wu D T, Chen B W, Mi M J, Wang Y L and Shen B 2024 *Chin. Phys. B* **33** 027503

[26] Kim Y S, Brahlek M, Bansal N, Edrey E, Kapilevich G A, Iida K, Tanimura M, Horibe Y, Cheong S W and Seongshik O 2011 *Phys. Rev. B* **2** 073109

[27] Lupke F, Pham A D, Zhao Y F, Zhou L J, Lu W C, Briggs E, Bernholc J, Kolmer M, Teeter J, Kolmer M, Teeter J, Ko W, Chang C Z, Ganesh P and Li A P 2022 *Phys. Rev. B* **105** 035423

[28] Wu X K, Wang B, Wu D T, Chen B W, Mi M J, Wang Y L and Shen B 2017 *Chin. Phys. B* **33** 027503

[29] Niu J J and Yan B M 2017 *Phys. Rev. B* **96** 075402

[30] Kar I, Routh S, Ghorai S, Purwar S and Thirupathaiah S 2023 *Solid State Commun.* **369** 115209

[31] Nakanishi M, Yoshimura K, Kosuge K, Goto T, Fujii T and Takada J 2000 *J. Magn. Magn. Mater.* **221** 301

[32] Dhara S, Chowdhury R R and Bandyopadhyay B 2016 *Phys. Rev. B* **93** 214413

[33] Singh M, Ghosh L, Gangwar V K, Kumar Y, Pal D, Shahi P, Kumar S, Mukherjee S, Shimada K and Chatterjee S 2022 *Appl. Phys. Lett.* **121** 032403

[34] Ghosh S, Tanguturi R G, Pramanik P, Joshi D C, Mishra P K, Das S and Thota S 2019 *Phys. Rev. B* **99** 115135

[35] Ghosh T, Fukuda T, Kakeshita T, Kaul S N and Mukhopadhyay P K 2017 *Phys. Rev. B* **95** 140401

[36] Wang J S, Powers W, Zhang Z, Smith M, McIntosh B J, Bac S K, Riney L, Zhukovskyi M, Orlova, T, Rokhinson L P, Hsu Y T, Liu X Y and Assaf B A 2022 *Nano Lett.* **22** 792

[37] Roulleau P, Choi T, Riedi S, Heinzel T, Shorubalko I, Ihn T and Ensslin K 2010 *Phys. Rev. B* **81** 155449

[38] Sasmal S, Mondal R, Kulkarni R, Thamizhavel A and Singh B 2020 *J. Phys.: Condens. Matter* **32** 335701

[39] Laha A, Singha R, Mardanya S, Singh B, Agarwal A, Mandal P and Hossain Z 2021 *Phys. Rev. B* **103** l241112

[40] Brinkman A, Huijben M, Van Zalk M, Huijben J, Zeitler U, Maan J C, Van der Wiel W G, Rijnders G, Blank D H A and Hilgenkamp H 2007 *Nat. Mater.* **6** 493

[41] Felsch W and Winzer K 1973 *Solid State Commun.* **13** 569

[42] Zhang Y H, Kahle S, Herden T, Stroh C, Mayor M, Schlickum U, Ternes M, Wahl P and Kern K 2022 *Nat. Commun.* **13** 5067

[43] Anderson P W 1970 *J. Phys. C* **3** 2436

[44] Gentile P, de Leo L, Fabrizio M and Tosatti E 2009 *Europhys. Lett.* **87** 27014

[45] Nagaosa N, Sinova J, Onoda S, MacDonald A H and Ong N P 2010 *Rev. Mod. Phys.* **82** 1539

[46] Liu E K, Sun Y, Kumar N, Muechler L, Sun A L, Jiao L, Yang S Y, Liu D F, Liang A J, Xu Q N, Kroder J, Süss V, Borrmann H, Shekhar C, Wang Z S, Xi C Y, Wang W H, Schnelle W, Wirth S, Chen Y L, Goennenwein S T B and Felser C 2018 *Nat. Phys.* **14** 1125

[47] Tanaka M, Fujishiro Y, Mogi M, Kaneko Y, Yokosawa T, Kanazawa N, Minami S, Koretsune T, Arita R, Tarucha S, Yamamoto M and Tokura Y 2021 *Nano Lett.* **20** 7476